Infrared surface polaritons on antimony

Justin W. Cleary,[1,*] Gautam Medhi,[2] Monas Shahzad,[2] Imen Rezadad,[2] Doug Maukonen,[2] Robert E. Peale,[2] Glenn D. Boreman,[3] Sandy Wentzell,[4] and Walter R. Buchwald[4]

[1]Sensors Directorate, Air Force Research Laboratory, Wright-Patterson Air Force Base, Ohio, 45433, USA
[2]Department of Physics, University of Central Florida, Orlando, Florida 32816, USA
[3]Department of Physics and Optical Science, University of North Carolina at Charlotte, Charlotte NC 28223, USA
[4]Solid State Scientific Corporation, Hollis, New Hampshire 03049, USA
[*]Justin.Cleary@WPAFB.af.mil

Abstract: The semimetal antimony, with a plasma frequency ~80 times less than that of gold, is potentially useful as a host for infrared surface polaritons (SPs). Relevant IR SP properties, including the frequency-dependent propagation length and penetration depths for fields into the media on either side of the interface, were determined from optical constants measured on optically-thick thermally-evaporated Sb films over the wavelength range 1 to 40 μm. Plasma and carrier relaxation frequencies were determined from Drude-model fits to these data. The real part of the permittivity is negative for wavelengths beyond 11 μm. Distinct resonant decreases in specular reflected intensity were observed for Sb lamellar gratings in the wavelength range of 6 to 11 μm, where the real part of the permittivity is positive. Both resonance angles and the angular reflectance spectral line shapes are in agreement with theory for excitation of bound surface electromagnetic waves (SPs). Finite element method (FEM) electrodynamic simulations indicate the existence of SP modes under conditions matching the experiments. FEM results also show that such waves depend on having a significant imaginary part of the permittivity, as has been noted earlier for the case of surface exciton polaritons.

© 2012 Optical Society of America

OCIS codes: (240.5420) Polaritons; (240.6690) Surface waves; (240.6680) Surface plasmons; (040.3060) Infrared; (350.2770) Gratings; (280.4788) Optical sensing and sensors.

References and links

1. A. Brillante, I. Pockrand, M. R. Philpott, and J. D. Swalen, "Experimental Observation of Exciton Surface Polaritons on a Polymerized Diacetylene Crystal," Chem. Phys. Lett. **57**(3), 395–399 (1978).
2. F. Yang, J. R. Sambles, and G. W. Bradberry, "Long-Range Surface Modes Supported By Thin Films," Phys. Rev. B Condens. Matter **44**(11), 5855–5872 (1991).
3. F. Yang, G. W. Bradberry, and J. R. Sambles, "Experimental Observation of Surface Exciton-polaritons on Vanadium using Infrared Radiation," J. Mod. Opt. **37**(9), 1545–1553 (1990).
4. R. Soref, R. E. Peale, and W. Buchwald, "Longwave plasmonics on doped silicon and silicides," Opt. Express **16**(9), 6507–6514 (2008).
5. J. W. Cleary, R. E. Peale, D. J. Shelton, G. D. Boreman, C. W. Smith, M. Ishigami, R. Soref, A. Drehman, and W. R. Buchwald, "IR permittivities for silicides and doped silicon," J. Opt. Soc. Am. B **27**(4), 730–734 (2010).
6. M. Shahzad, G. Medhi, R. E. Peale, W. R. Buchwald, J. W. Cleary, R. Soref, G. D Boreman, and O. Edwards, "Infrared surface plasmons on heavily doped silicon," J. Appl. Phys. **110**(12), 123105 (2011).
7. J. C. Ginn, R. L. Jarecki, Jr., E. A. Shaner, and P. S. Davids, "Infrared plasmons on heavily-doped silicon," J. Appl. Phys. **110**(4), 043110 (2011).
8. H. Raether, "Surface plasma oscillations and their applications," in *Physics of Thin Films* (Academic Press, New York, 1977) **9**, 145–261.
9. J. W. Cleary, G. Medhi, R. E. Peale, and W. R. Buchwald, "Long-wave infrared surface plasmon grating coupler," Appl. Opt. **49**(16), 3102–3110 (2010).
10. P. Halevi, in *Electromagnetic Surface Modes*, A. D. Boardman, ed. (Wiley, Chichester, 1982).
11. M. G. Cottam and D. R. Tilley, *Introduction to Surface and Superlattice Excitations,* (Cambridge Univ. Cambridge UK, 1988).
12. E. B. Sernelius, *Surface modes in Physics*, (Wiley-Vch, Berlin, 2000).

13. H. Raether, *Surface Plasmons on Smooth and Rough Surfaces and on Gratings* (Springer, New York, 1988).
14. K. Welford, "Surface plasmon-polaritons and their uses," Opt. Quantum Electron. **23**(1), 1–27 (1991).
15. A. Hessel and A. A. Oliner, "A new theory of Wood's anomalies on optical gratings," Appl. Opt. **4**(10), 1275–1297 (1965).
16. L. D. Landau, E. M. Lifshitz, and L. P. Pitaevskii, *Electrodynamics of continuous media*, Course of theoretical physics vol. 8 (Butterworth-Heinenann, Oxford, 2002), Sect. 87.
17. E. B. Saff and A. D. Snider, *Fundamentals of complex analysis with applications to engineering and science,* 3rd ed. (Pearson Education,Upper Saddle River, New Jersey, 2003).
18. P. Y. Yu and M. Cardona, *Fundamentals of Semiconductors* (Springer, Berlin, 1996).
19. H. G. Tompkins and E. A. Irene, *Handbook of Ellipsometry* (William Andrew, Heidelberg, 2005).
20. T. J. Fox, R. P. Howson, and D. C. Emmony, "Optical properties of thin films of antimony," J. Phys. D Appl. Phys. **7**(13), 1864–1872 (1974).
21. L. Harris and F. R. Corrigan, "Optical and electrical properties of antimony deposits," J. Opt. Soc. Am. **54**(12), 1437–1441 (1964).
22. I. N. Shkliarevskii, A. A. Avdeenki, and V. G. Padalka, "Measurements of the Optical Constants of Antimony in the Infrared Region of the Spectrum at Temperatures of 290° and 110°," Opt. Spectrosc. **6**, 336 (1959).
23. J. W. Cleary, G. Medhi, R. E. Peale, W. Buchwald, O. Edwards, and I. Oladeji, "Infrared surface plasmon resonance biosensor," Proc. SPIE **7673**, 767306, 767306-11 (2012).
24. J. W. Cleary, R. E. Peale, D. Shelton, G. D. Boreman, R. Soref, and W. Buchwald, "Silicides for infrared surface plasmon resonance biosensors," Proc. MRS **1133**, 1133-AA10-03 (2008).

1. Introduction

Surface polaritons are electromagnetic waves coupled to surface polarization and are described by the equations of macroscopic electrodynamics [1–3]. They have been studied extensively in the visible and infrared wavelength region on semiconductors [4–7] and metals [8, 9]. Different types of surface polarization may be involved, including plasmon, phonon, magnon, and exciton [1–3]. Electrodynamic characteristics of these SPs, such as dispersion, energy propagation length, and field penetration depth, have identical formulation in terms of their wave function and the complex permittivities (or permeabilities) of the media on either side of the interface [10]. The characteristic optical excitation of SPs utilizing the surface electric polarization is via an incident p-polarized electric field with a field vector that lies in the plane containing the surface normal and the SP propagation wavevector.

It is commonly asserted that a surface *plasmon* polariton can be excited at a conductor/dielectric interface only when the conductor has a negative permittivity [8] provided that the absolute value of the conductor's permittivity significantly exceeds the positive permittivity of the dielectric. These conditions are most clear when the permittivities of both media are entirely real. However, these conditions for sustaining a surface plasmon polariton are not absolute [2, 3]. In fact, as long as the permittivity of the conductor is complex, a non-radiative surface mode may exist over the entire frequency range regardless of the sign of the real part since all associated wavevectors will also be complex [2]. Whether the mode is propagating or not and how quickly it decays in each medium away from the interface can be determined by the values of the real and imaginary components of all associated wavevectors. Bound surface waves that exist when the real part of the permittivity is small and positive, while the imaginary part exceeds the real part are known [2]. Different types of surface modes that depend on different types of surface polarization and different relations between real and imaginary parts of the permittivity are discussed in [10–14].

This work presents a determination of relevant IR SP properties for the semimetal Sb, including the frequency-dependent propagation length and penetration depths for the fields into the media on either side of the interface. These properties are calculated using optical constants that were measured over the wavelength range 1 to 40 µm on optically thick Sb. Plasma and carrier relaxation frequencies are determined from Drude-model fits to these data.

The optical excitation of SPs in this material is verified experimentally by considering the angular dependence of reflection from lamellar gratings. Interestingly, distinct absorption resonances consistent with SP generation are experimentally observed in these angular reflection spectra at wavelengths where the real part of the complex permittivity is positive. These absorption resonances are found to be consistent with standard analytical theory that

predicts a bound surface wave and with commercial finite element method (COMSOL-FEM) simulations that provide strong confirmation of such waves. These SP modes disappear in the simulations when the imaginary part of the complex permittivity is artificially zeroed, supporting the condition of having a sufficiently large imaginary part [2] for their appearance.

SP modes on Sb are a potential means of information transport in future nanophotonic devices due to tighter IR SP field confinement when compared to plasmon hosts such as noble metals. Their most significant potential commercial application is in biosensors, where the time dependent change in the resonant coupling of light to SPs gives information on binding and interactions of biomolecules to a suitably functionalized surface. The resonances reported here are potentially useful for this IR sensor application. Sensor applications simply require the existence of a suitable resonance that is sensitive to changes in the dielectric permittivity at the interface with the conductor.

2. Theoretical considerations

The p-polarized (TM) surface polaritons at a dielectric-metal interface are described by their magnetic field wave functions, which can be written as

$$H_y = H_o \, Exp\left[i\left(K_{sp}x - K_{zd,zc}|z| \right) \right],$$ (1)

where the complex surface polariton propagation vector along the interface (x-direction) K_{SP} is [3]

$$K_{SP}(\omega) = \frac{\omega}{c}\sqrt{\frac{\varepsilon_d \, \varepsilon_c}{\varepsilon_d + \varepsilon_c}} \, .$$ (2)

Here ε_d and ε_c are the complex permittivities of the dielectric and conductor, respectively. The complex wavevector of the surface polariton in the direction perpendicular to and on either side of the interface is given by

$$K_{zd,zc} = \sqrt{K_{SP}^2 - \varepsilon_{d,c}\left(\frac{\omega}{c}\right)^2} \, ,$$ (3)

where K_{zd} refers to the dielectric region with $z > 0$ (above the interface into the dielectric) and K_{zc} the conductor region $z < 0$. For traditional surface plasmon polariton hosts, such as gold at frequencies below its plasma frequency, we have Re[K_{SP}] >> Im[K_{SP}], which results in a bound surface wave propagating along the interface. Also in this traditional case, Im[$K_{zd,zc}$] >> Re[$K_{zd,zc}$] below the plasma frequency resulting in rapid exponential decay of the electromagnetic fields in the direction perpendicular to the interface. Above the plasma frequency, on the other hand, Re[$K_{zd,zc}$] >> Im[$K_{zd,zc}$] leading to the propagation of energy away from the interface. For the semi-metal Sb discussed here, Re[K_{SP}] ~ Im[K_{SP}] and Re[$K_{zd,zc}$] ~Im[$K_{zd,zc}$] leading to a situation where surface waves at frequencies both above and below the plasma frequency have similar characteristics.

Knowledge of the decay length for propagation of energy and the penetration depth for the field into the media on either side of the interface is important for determining how useful a particular conductor is for various applications. The energy decay length (1/2 of the electric field decay length) in the direction of propagation [8] is given by

$$L_x = \frac{1}{2 \, \text{Im}\left(K_{SP}(\omega) \right)} \, .$$ (4)

The 1/e penetration depth of the surface polariton fields [8] into the dielectric, L_d, or into the conductor, L_c, is given by

$$L_{d,c} = \left[\frac{\omega}{c} \text{Im} \sqrt{\frac{\varepsilon_{d,c}^{\ 2}}{\varepsilon_d + \varepsilon_c}} \right]^{-1}. \tag{5}$$

For traditional surface plasmon polariton hosts, at frequencies below the material's plasma frequency, K_{SP} exceeds the wavevector of a freely propagating optical field at the same frequency and as such there can be no direct excitation of SP modes from optical fields. When $\varepsilon_c' > 0$, K_{SP} is less than the wavevector of a freely propagating optical field, i.e. the SP dispersion curve lies above the grazing-incidence light line and thus no momentum matching device (prism or grating) is required to excite such SPs. For Sb, the SP dispersion lies very close to the grazing-incidence light line at all frequencies, but grazing incidence is experimentally impractical for the excitation of SPs and observation of their effects. To alleviate this problem, a grating coupler can be used to allow for a more convenient angle of incidence. The coupling condition [8, 9] between an electromagnetic wave, which is incident from the dielectric at an angle θ onto a conducting grating, and a SP is given by

$$\sin(\theta) + \frac{m\lambda}{p} = \pm \frac{c}{\omega} \text{Re}[K_{SP}], \tag{6}$$

where p is the grating period, m is an integer of either sign, and λ is the excitation wavelength. Our experiment considers only positive angles of incidence θ.

Angular reflection spectra associated with the excitation of SP modes can be described using the analytical theory of Hessel and Oliner [15], which predicts absorption resonances that are accompanied by surface waves with wavefunctions given by Eq. (2). We adopt the simplifying assumption that the grating is represented by a sinusoidal surface impedance [9]. Only the first order resonance ($m = 1$) appears in this case, but this suffices to characterize the photon-to-SP resonant coupling. The theory of Hessel and Oliner gives the specular reflection from a grating, R, in the form

$$R \approx \left[abs \left(1 - \frac{4\cos\theta}{M\zeta \left(D_0 - D_1^{-1} - D_{-1}^{-1} \right)} \right) \right]^2. \tag{7}$$

where M is the unitless amplitude of the sinusoidal impedance modulation [9, 15], ζ is the spatial-average surface impedance relative to the impedance of free space (377 Ω) and the coefficients D with a subscript integer s are given by

$$D_s = \frac{2}{M} \left[1 + \frac{1}{\zeta} \sqrt{1 - \left(\sin\theta + \frac{s\lambda}{p} \right)^2} \right]. \tag{8}$$

With $\zeta = 1/\sqrt{[\varepsilon_c]}$ and $\varepsilon_c' = \varepsilon_c' + i\,\varepsilon_c''$ we obtain

$$\zeta = \begin{bmatrix} -i \\ 1 \end{bmatrix} \left(\varepsilon_c'^2 + \varepsilon_c''^2 \right)^{-1/4} \left\{ \cos\left(\frac{\phi}{2} \right) - i\sin\left(\frac{\phi}{2} \right) \right\} \quad for \quad \begin{matrix} \varepsilon_c' < 0 \\ \varepsilon_c' > 0 \end{matrix}, \tag{9}$$

where $\phi = \tan^{-1}(\varepsilon_c''/\varepsilon_c')$. On physical grounds we always require $\text{Re}[\zeta] > 0$ and $\text{Im}[\zeta] < 0$ [16] which determines the coefficient of the fourth root in Eq. (9) from four possible pre-factors ($\pm$ 1, $\pm$ i) [17]. Finally, to compare experimental reflection data to the theory of Hessel and Oliner in this work, M, which is an unspecified function of grating permittivity, amplitude and wavelength, is varied to obtain the best match to the measured data. This qualitative approach to fitting gives an M value which is accurate to within ~10%.

In general, the aforementioned wave vectors (K_z and K_{SP}) completely describe the SP with the complex nature of these functions arising primarily from the complex nature of ε_c. In the

region of negative permittivity where free carriers dominate, ε_c takes the Drude form of [5,18]

$$\varepsilon_c = \varepsilon_c' + i\varepsilon_c'' = \varepsilon_\infty \left[1 - \frac{\left(\omega_p{}^2 / \omega^2 \right)}{1 + i\left(\omega_\tau / \omega \right)} \right],$$ (10)

where ω_p and ω_τ are the bulk plasma and electron relaxation frequencies respectively and ε_∞ is the permittivity of the material at frequencies well above the bulk plasma frequency. Equation (10) is used in this work to extract these Drude parameters for Sb from empirical data.

3. Experimental details

Antimony films were thermally evaporated from 99.999% pure Sb pellets onto various substrates. The film thickness was monitored during evaporation using a crystal monitor. Double-side polished high-resistivity silicon substrates allowed transmittance measurements using a Bomem DA8 Fourier spectrometer with a globar source, KBr beamsplitter, and HgCdTe detector to determine the IR penetration depth. This information was used to insure that the films subsequently prepared for ellipsometry measurements were optically thick. An Sb film deposited on a glass slide was characterized using a J.A. Woollam IR-VASE ellipsometer in the wavelength range of 1 - 40 μm. The raw ellipsometer output was used to calculate the complex permittivity spectrum using standard Fresnel equations [19].

Lamellar gratings of 20 μm period, 50% duty cycle and different amplitudes were formed by photolithography and plasma etching in silicon. Figure 1 (left) presents scanning electron microscope images of one such patterned silicon substrate. An optically thick Sb layer was then deposited on these structures, and Fig. 1 (center) presents an SEM image of such a sample. The subsequent morphology was measured using a step profilometer, and a measured profile is presented in Fig. 1 (right).

Specular reflectance as a function of incidence angle was obtained for the antimony gratings using either quantum cascade lasers (QCLs) at 9.38 or 6.14 μm wavelengths, or a CO_2 laser tuned to 9.250 or 10.591 μm wavelength. The QCL multimode lasers have bandwidths of 0.16% and 0.20% for the 6.14 or 9.38 μm wavelengths, respectively. Either a 77 K, HgCdTe detector (for the QCL) or a power meter (for the CO_2 laser) was used to detect the reflected light. In all cases, the laser radiation was p-polarized, i.e. with the electric field vector in the plane of incidence. The grating samples and detector were mounted on the θ and 2θ parts of a motorized goniometer, respectively. SP generation was observed as a resonant decrease in the reflected intensity at certain angles. A schematic of the experiment is shown in Fig. 1 (right).
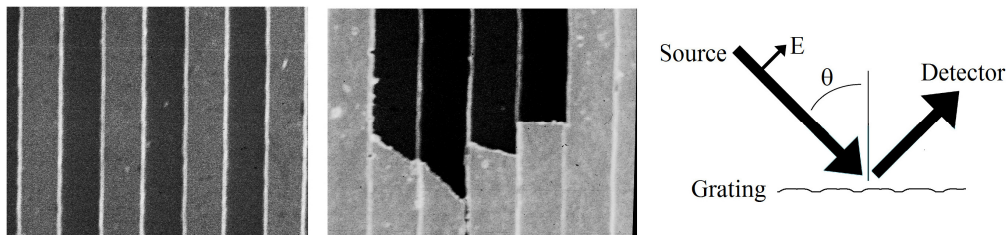

Fig. 1. (left) Scanning electron microscope image of a silicon grating substrate with 50% duty cycle, 20 μm period and 1 μm amplitude. (center) Sb-coating on the same grating structure with the coating partially removed in upper central region. (right) Schematic of SP experiments completed in this work. The sources used were a CO_2 and quantum cascade lasers with incident light being p-polarized as indicated by *E*. A power meter and a HgCdTe detector were used to measure the specular reflection from the grating as a function of *θ*. The measured profile pictured is of a 2-μm-amplitude Sb coated grating.

4. Results

The complex permittivity spectrum, determined from ellipsometry and plotted in Fig. 2, agrees reasonably with previously published results for bulk Sb [20, 21] and for a ~160 nm thick film [22]. These prior results are also plotted in Fig. 2 for comparison. Our data show that ε' crosses from positive to negative values at a wavelength of 11.1 μm. The crossing point for the data of reference [21] is the same. The crossing points for Refs [20] and [22] lie at 11.6 and 10 μm, respectively. The imaginary part of the permittivity is significantly larger than the magnitude of the real part at CO_2 laser wavelengths, and they are comparable to each other at 6.14 μm. This is similar to the conditions for the surface exciton polaritons observed in [2], and is in contrast to the usual situation for surface plasmon polaritons on ordinary metals at visible wavelengths where $|\varepsilon_c'| \gg \varepsilon_c''$. The empirical permittivity and relative surface impedance values to be used in this work are presented in Table 1.

Transmittance spectra, T, of two Sb films having thicknesses d of 340 and 680 nm, deposited on Si substrates, were measured. The IR penetration depth was found from $\delta = 2(d_2-d_1)/\ln(T_1/T_2)$. These values are compared with values calculated from the permittivity using $\delta = c/\omega\ \mathrm{Im}[\sqrt{\varepsilon}]$. Near a wavelength of 8 μm, the maximum penetration depth is ~570 nm, which is a factor of 2 smaller than the thickness of the films deposited for the ellipsometry and grating experiments (1.15 and 1.19 μm, respectively). Thus, we consider that the ellipsometry results give information mainly on bulk Sb with little influence from the glass substrate.
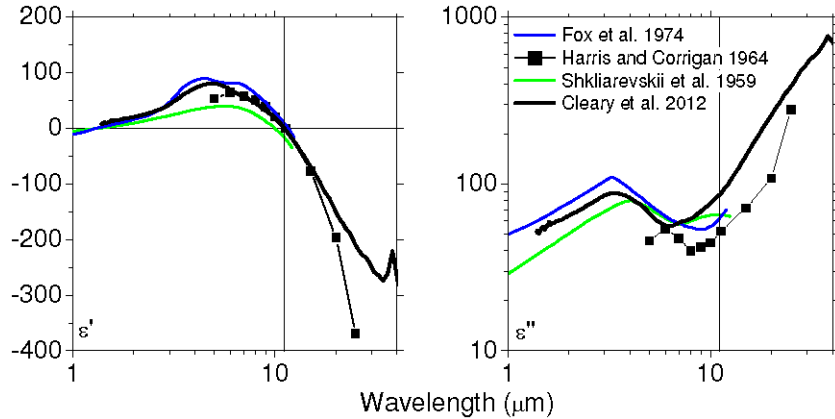

Fig. 2. (left) Real part of permittivity for Sb. (right) Imaginary part. The prior measurements are from References [20–22]. The vertical line indicates the zero crossing of the real part of the permittivity.

Table 1. Empirical Optical Parameters of Sb for the Four Laser Wavelengths Used

λ (μm)	ε'	ε''	ζ
6.14	68.1	56.0	0.100-i(0.036)
9.250	28.3	70.8	0.095-i(0.064)
9.38	26.4	71.9	0.094-i(0.065)
10.591	8.49	82.0	0.082-i(0.074)

Drude constants were extracted by fitting Eq. (10) to the measured complex permittivity spectrum for wavelengths in the range 15 to 30 μm where the ellipsometry data is Drude-like. An apparent artifact near 40 microns was not included in the fit. Over this range, the Drude fit differs from our plotted permittivity curve by less than the plotted line thickness. The values for the constants obtained are $\omega_p = 0.134 \pm 0.005$ eV, $\omega_\tau = 0.060 \pm 0.003$ eV, and $\varepsilon_\infty = 105 \pm 10$. This plasma frequency is 20% larger than the frequency at which ε' is observed to change sign, but the permittivity already deviates significantly here from Drude like behavior. The obtained values for ω_p and ε_∞ are within 25% of those from Refs [20, 21]. The obtained value for ω_τ is 3x larger than that from Ref [20], a difference possibly due to a difference in the

microsctructure of our film. Since the experiments discussed in this work occur in regions of positive permittivity where the Drude model is invalid, all calculations relevant to SPs in this work are based on empirical permittivities.

Figure 3 presents the difference between the grazing incidence light line, $k = \omega/c$ and $Re[K_{SP}]$, Eq. (2), for Sb. The laser wavelengths used in the experiments are indicated by vertical dashed lines. Since ω_τ is not small compared with ω_p, unlike the case for traditional SP hosts, the polariton nature of the dispersion curve, namely the usual inflection near $\omega = \omega_p / \sqrt{2}$, is scarcely noticeable, except in this difference spectrum. The negative data define the region of usual surface plasmon polaritons corresponding to negative ε_c'. In contrast, our experiments on excitation of surface polaritons using Sb gratings occur in the region of positive ε_c' or positive data in Fig. 3.
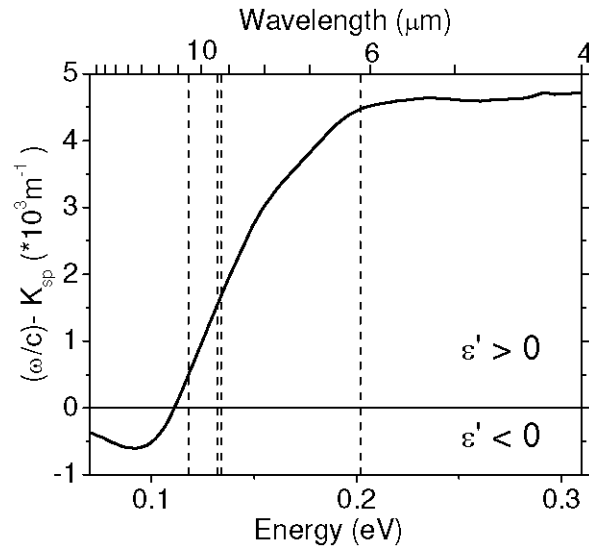

Fig. 3. Difference between grazing incidence light line and the SP dispersion curve for Sb as calculated from empirical permittivities. Laser wavelengths used in this work are indicated by vertical dashed lines. Positive y-axis values indicate positive permittivity values.

Measured profiles of the antimony gratings indicate grating amplitudes of 0.54 ± 0.04, 1.05 ± 0.06, and 2.0 ± 0.1 µm. The duty cycle of the raised ridges exceeds the 50% duty cycle of the bare patterned Si substrate, and the corners are more rounded, showing that the groove side walls are also coated with Sb to form a continuous conducting film (Fig. 1). The 2 µm amplitude grating gives duty cycles approaching $74 \pm 4\%$ with Sb coating while the shorter gratings give values closer to the nominal 50% duty cycle. Our experiments with lamellar gratings formed by gold strips on bare silicon have shown that SP-related resonances are only observed when the metal film is continuous. We use the nominal 20 µm period of the mask and 50% duty cycle where applicable in analytical or FEM calculations.

Figure 4 presents angular reflection spectra of Sb gratings using two QCLs and two CO_2 laser wavelengths. The Sb films deposited were optically thick, according to the earlier skin depth determination, so that the results presented here are due to a bulk Sb grating with no influence from the underlying silicon. The values plotted are normalized reflected intensity. Spectra for different grating amplitudes are offset vertically by unity for clarity. Resonances due to excitation of SPs appear clearly for grating amplitudes of at least 0.5 µm. Calculated resonance angles from Eq. (6) are indicated by symbols.

In the theory of Hessel and Oliner [15], absorption resonances in grating reflectivity occur due to excitation of bound electromagnetic surface waves. Calculated curves according to this theory are plotted in Fig. 4 as heavy lines adjacent to the corresponding experimental data.

The theory curves have been shifted vertically by amounts necessary to avoid overlapping the experimental curves. Except for the sharp upward spikes at the highest grating amplitudes, the calculated resonance spectra from Eq. (7) represent resonance positions, strengths, and widths in fair agreement with the observations. The agreement in angular position is better for the data from the CO_2 laser because of its superior beam quality and intensity which more accurately defines the angle of incidence. The similarity in experimental and calculated resonance spectra supports the interpretation that creation of bound surface waves is responsible for the resonances. Angular reflection spectra for uncoated silicon gratings show no resonances [6], additionally supporting the interpretation that the observed resonances are due to the excitation of bound SPs on antimony.
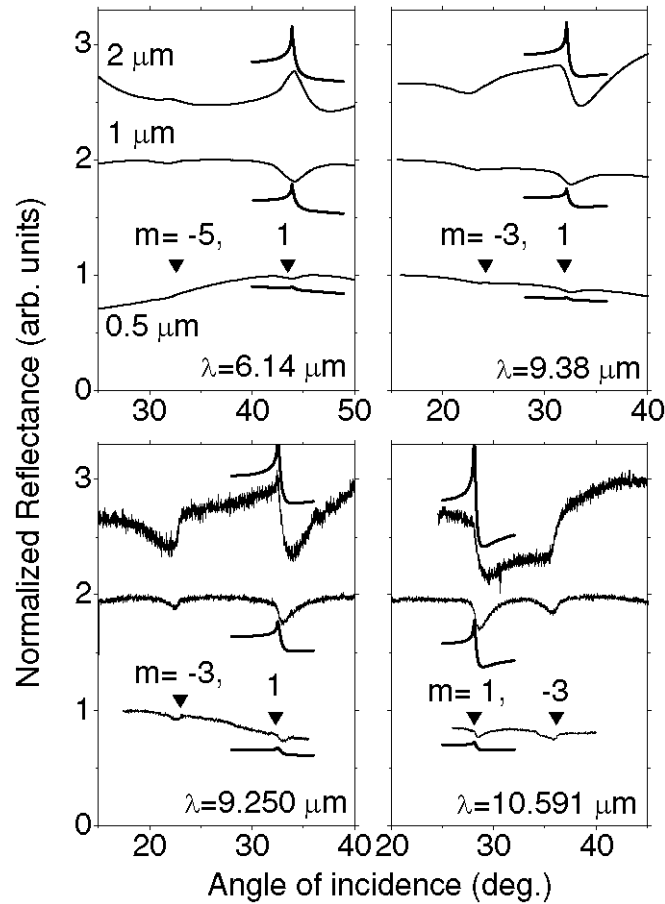

Fig. 4. Angular reflectance spectra of Sb gratings at QCL and CO_2 laser wavelengths. Smooth curves are calculated reflectance spectra. Grating amplitudes used (from the top) were 2, 1, and 0.5 μm.

FEM simulations (COMSOL Multiphysics) support the interpretation of resonant excitation of bound SP waves on antimony, even when $\varepsilon_c' > 0$, provided that ε_c'' is sufficiently large. Figure 5 presents contour plots of the electric field distribution in the case of an incident polarized field with a specified λ and θ on an antimony grating. Figure 5 (upper) is for the case of the photon frequency below the plasma frequency, such that that $\varepsilon_c' < 0$, the usual condition for surface plasmon polariton excitation. Figure 5 (lower) is for the opposite regime, where $\varepsilon_c' > 0$. The incident angles used were chosen to match the first order resonance condition according to Eq. (6), or 23.6° and 28.1° for 12 and 10.6 μm wavelengths,

respectively. The grating profile was lamellar as in our experiments, with an amplitude of 2 μm. The portion of the surface pictured in Fig. 5 lies 250 μm to the right of the grating in order to clearly illustrate SP modes without interference from other features such as incident and diffracted beams. The field distribution is similar in both cases, showing rapid decay away from the surface, as appropriate for a bound wave. The wavelength along the surface is essentially the same as the incident IR wavelength, as expected for a SP whose dispersion is close to the light line, as is the case for Sb (Fig. 3). Two maxima belong to each SP period in Fig. 5, because the magnitude of the electric field components is plotted. The field strengths are ~3 x smaller at the shorter wavelength, but otherwise the behavior is the same above and below the ε' sign change.
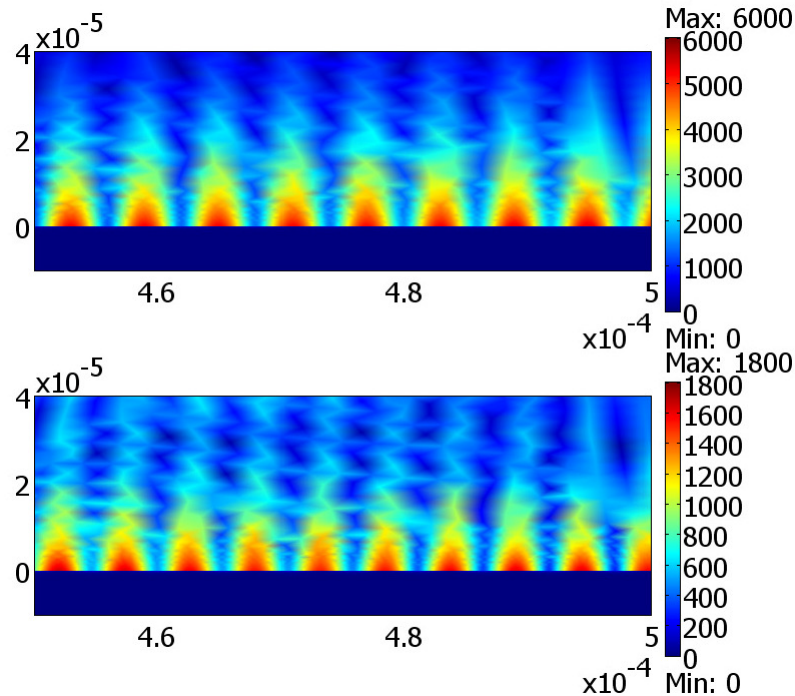

Fig. 5. Spatial electric field magnitude in [V/m] of surface polaritons on an antimony grating for incident photons of wavelengths of 12 μm (upper) and 10.6 μm (lower), which fall into the regimes of $\varepsilon_c' < 0$ and $\varepsilon_c' > 0$, respectively. The incident light falls on a grating of finite width (250 μm outside the plot to the left) with a period of 20 μm, 50% duty cycle, and 2 μm amplitude. The SP modes pictured are calculated for the first order resonances occurring at incidence angles 23.6° and 28.1°, respectively. The axes units are meters.

In comparison to Fig. 5, the plots in Fig. 6 cover an 8x broader horizontal scale, a 2.7x larger vertical scale, and have a different color field-strength scales. The grating is observed on the surface in the 0-200 μm horizontal range. Light is incident from the upper left on the grating and can be observed leaving the surface in several diffraction orders. The conditions for Fig. 6 (upper) are the same as in Fig. 5 (lower), i.e. the actual complex permittivity (where the imaginary part significantly exceeds the positive, real part) and the angle of incidence for exciting the first order SP (28.1°), according to Eq. (6). Bound surface waves are clearly visible propagating toward the right along the interface. These wave fronts are nearly orthogonal to the surface, and the field strength decays along the surface with a characteristic decay length of order 100 μm while the field decays away from the surface with a characteristic length of ~10 s of microns. The out-coupled diffraction orders observed are $m = 0$ (specular), $m = 1$ (propagating toward the middle of the right boundary), and $m = -3$

(propagating toward the middle of the left boundary). The incident beam appears weaker relative to the other plots in Fig. 6 due to the comparative intensity of the SP fields in Fig. 6 upper.

If ε_c'' is artificially set to zero, we obtain the FEM results presented in Fig. 6, middle and lower. Excitation of the first order SP should occur at nearly the same angle of incidence (within 0.3%) as the first order "Rayleigh anomaly" [9, 15], where the first order diffracted beam exits the half-space above the surface at grazing incidence. The $m = 1$ diffracted beam that propagates toward the middle of the right border in Fig. 6 (upper and lower) becomes this grazing beam if the angle of incidence is reduced by just 0.1 deg to the value 28.0°. FEM simulations performed at this angle, however, do not show the intense clear wave fronts that were observed hugging the surface in Fig. 6 (upper).

Figure 6 (middle) shows that zeroing ε_c'' eliminates the bound SP wave when the angle of incidence is the same as in Fig. 6 (upper). The range of the color scale has decreased 5 x in comparison to Fig. 6 (upper) so that now the incident beam is the most intense feature. This emphasizes the absence of an SP in Fig. 6 (middle) and the intensity of the SP fields in Fig. 6 (upper).

To be fair, artificially zeroing the imaginary part of the permittivity also affects the SP excitation resonance angle, according to Eq. (6). Thus, fair comparison requires that the simulation be performed at this new angle, which is 24.6°. A simulation performed at this angle also indicates the absence of SP modes, as shown in Fig. 6 (lower). At this smaller angle, the first order diffracted beam has moved further away from grazing incidence as expected. As with Fig. 6 (middle), in Fig. 6 (lower) the incident beam and first order diffracted beam dominate and are at comparable (low) intensities for the two plots. The appearance of SP modes in Fig. 6 (upper) and the lack of any features resembling bound electromagnetic modes in Fig. 6 (lower) support the assertion that bound SP modes may occur when $\varepsilon_c' > 0$ if ε_c'' is sufficiently large. These FEM results lend additional support to the interpretation that the observed resonances in Fig. 4 are due to the excitation of bound SPs.
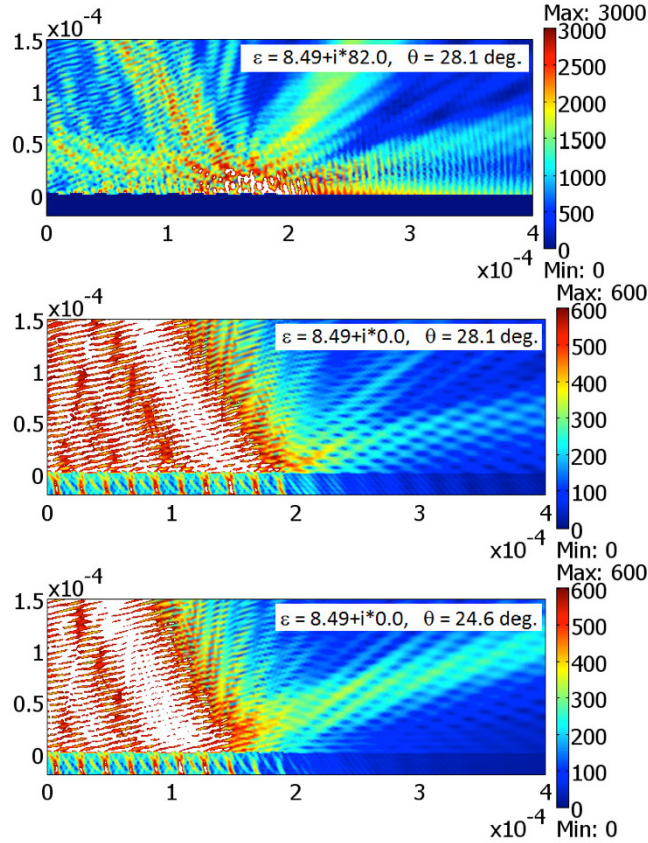
Fig. 6. Spatial electric field magnitude in [V/m] of surface polaritons on an antimony grating at a wavelength of 10.6 μm. The grating has a period of 20 μm, with a 50% duty cycle and 2 μm amplitude. The SP modes pictured are calculated using a complex permittivity at 28.1° incidence (upper), real permittivity at 28.1° (middle), and real permittivity at 24.6° (lower). Axes units are meters.

The SP energy decay length or propagation length, L_x, is determined from Eq. (4) and is presented in Fig. 7 (left) as a function of free-space photon wavelength. A broad shallow dip for Sb occurs near 11 μm where ε' changes sign. The propagation length is similar on either side of this transition and the characteristic length of ~100 μm near 10 μm wavelengths is comparable (within the expected factor of 2) to the electric field decay length along the interface from the FEM calculations pictured in Fig. 6 (upper).

The characteristic penetration of the SP electric field into the dielectric (in this case air) and into the conducting film were determined by Eq. (5) and are presented in Fig. 7 (right) as functions of free space wavelength for antimony. The penetration depth into air is approximately twice the wavelength in the CO_2 laser range. Note that the penetration depths for Sb differ little on either side of the 11 μm wavelength where ε_c' changes sign. This is already indicated by Fig. 5, where the spatial extent of SP modes differs little on each side of the plasma wavelength (~11 μm). Inflections are observed near the ε_c' sign change similar to Fig. 7 (left). Both the analytical results (Fig. 7 right) and FEM results (Fig. 5) agree with mode penetration depths on the order of 10 μm near the experimental wavelengths.
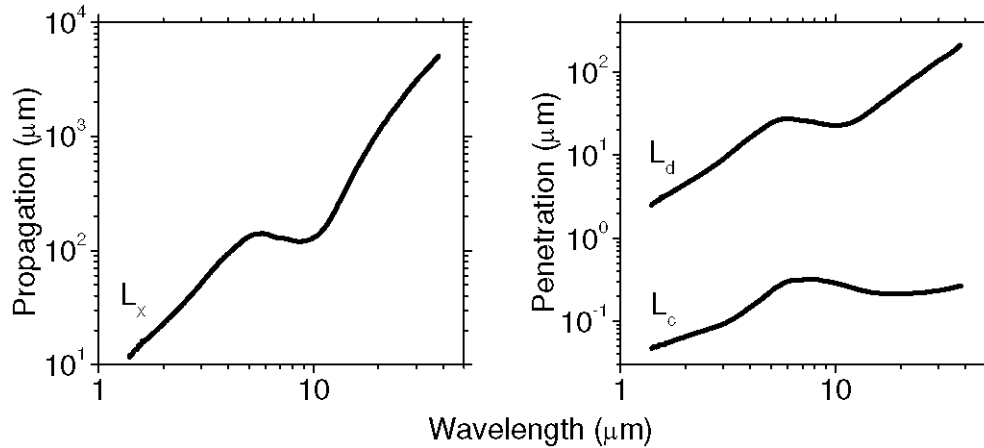
Fig. 7. Surface polariton properties for antimony. (left) Energy propagation length as a function of free space wavelength. (right) Field penetration depths versus free space wavelength. Upper curves show penetration depth into air while the lower curves show penetration depth into the conductor.

5. Discussion

The traditional conditions for surface plasmon polariton excitation requires $\varepsilon_c' < 0$ and $|\varepsilon_c'| >> \varepsilon_c''$ [4,8]. We present evidence that bound surface polaritions, which are similar in all respects to surface plasmon polaritons, occur on Sb at wavelengths where ε_c' is small but positive and ε_c'' is sufficiently large.

For an "ideal" metal, with zero ε_c'', and at frequencies where ε_c' is negative, K_z would be pure imaginary and the SP bound. At frequencies with positive permittivity, K_z would be purely real and the SP unbound. For Sb, K_z, or Eq. (3), has real and imaginary components of the same order of magnitude on either side of the permittivity sign change, and it varies slowly and monotonically with no discontinuities in the real or imaginary parts throughout the 2 to 40 μm wavelength range of our permittivity measurements. Hence, the SPs appear bound on both sides of the sign change with little to distinguish them (Figs. 5 and 7). Clear resonances are observed in the angular reflectance spectra (Fig. 4). These resonances are attributable to SPs on Sb since similar measurements on uncoated silicon gratings yield no resonances unless the carrier concentration exceeds ~1x10^{20} cm^{-3} [4, 6]. This SP interpretation is supported by analytic and FEM calculations. FEM results shown here indicate that a sufficiently large imaginary part of permittivity is required if the permittivity is positive in order to excite SPs.

Sensor applications mainly require the existence of a SP resonance that is sensitive to index changes above the grating. Based on the results shown here that indicate the presence of SPs on Sb, this semimetal may be useful for mid- to long-wavelength infrared sensing. The potential advantage of a molecular sensor that operates in the IR is the opportunity to operate near characteristic vibrational absorption lines [23, 24] where selectivity would be enhanced, and the dispersion of the refractive index would allow for a larger index change and hence improved sensitivity.

It may be useful to compare SP properties of Sb to other materials that have IR plasma frequencies. Silicon based materials (metal silicides and highly doped-Si) have been investigated recently in the mid- to long-wave IR wavelength regimes [4–7]. The SP propagation length on Sb at a wavelength of 10 μm is approximately 20 times smaller than on metal silicides [5] while the SP mode is about 250 times more tightly confined for Sb than it is for metal silicides. At smaller wavelengths (~5 μm) the metal silicides are comparable to Sb. The mode confinement on Sb is comparable to that of highly doped-Si [4–7] with carrier

concentrations near $\sim 10^{21}$ cm^{-3}. Lower concentrations of doped-Si do give slightly better mode confinement than Sb although the useful doping range is narrow, since silicon shows no SP resonances at CO_2 wavelengths below concentrations of 10^{20} cm^{-3} [6]. Thus Sb may be a more versatile material for IR SP-based sensing than silicon.

In summary, this paper reports the observation of SP resonances in the experimental and calculated angular reflection spectrum from Sb grating couplers. These resonances appear even though the real part of the permittivity is positive. These resonances in the wavelength range 6-11 μm are distinct and potentially useful for sensor applications. Antimony may also be useful for IR SP waveguide applications, though the mode confinement is no better than twice the photon wavelength at any frequency.

Acknowledgments